DESIGN AND BEHAVIOR OF POST-TENSIONED STEEL MOMENT FRAMES

Maria GARLOCK[1], Richard SAUSE[2], James M. RICLES[3]

SUMMARY

Steel moment resisting frames with post-tensioned (PT) connections use post-tensioned high strength strands running parallel to the beam to compress the beam flanges against the column flange. The post-tensioning produces a resisting moment to service loading and provides a restoring force that returns the frame to its pre-earthquake position. The behavior and design of a PT connection and PT frame *system* is described, where a PT frame system is a PT frame interacting with the floor system. It is shown that (1) frames with PT connections "expand", and this expansion requires that the floor system be designed to accommodate the expansion, and (2) the interaction of the floor system with the PT frame produces axial forces in the beams that add to those caused by post-tensioning. This paper proposes a performance based design approach for steel PT frame systems. Seismic performance levels, seismic input levels, structural limit states, and the structural demands for a PT frame system are defined. The design objectives are outlined, design criteria are proposed, and a step-by-step design procedure is given for PT frame systems. The proposed design approach is evaluated via comparisons with time-history analysis results for PT frame systems.

INTRODUCTION

A typical welded moment connection for a steel moment resisting frame (MRF) consists of a bolted shear tab with full penetration beam flange welds. During the 1994 Northridge earthquake, many steel MRFs suffered unexpected weld fractures, which diminished the strength and ductility of these connections. Several alternative moment connection details have been proposed since the Northridge earthquake [1] in an attempt to develop ductile response under earthquake loading. These details are intended to avoid weld failure and force inelastic deformation to develop in the beams away from the welds. However, as a result of these inelastic deformations (yielding and local buckling), the beams with these connections will suffer permanent damage under the design level earthquake. This damage can result in a significant residual drift of a MRF.

---

[1] Assistant Professor, Dept. of Civil and Environmental Engineering, Princeton University
[2] Joseph T. Stuart Professor of Structural Engineering, ATLSS Center, Dept. of Civil and Environmental Eng., Lehigh University
[3] Bruce G. Johnson Professor of Structural Engineering, ATLSS Center, Dept. of Civil and Environmental Eng., Lehigh University
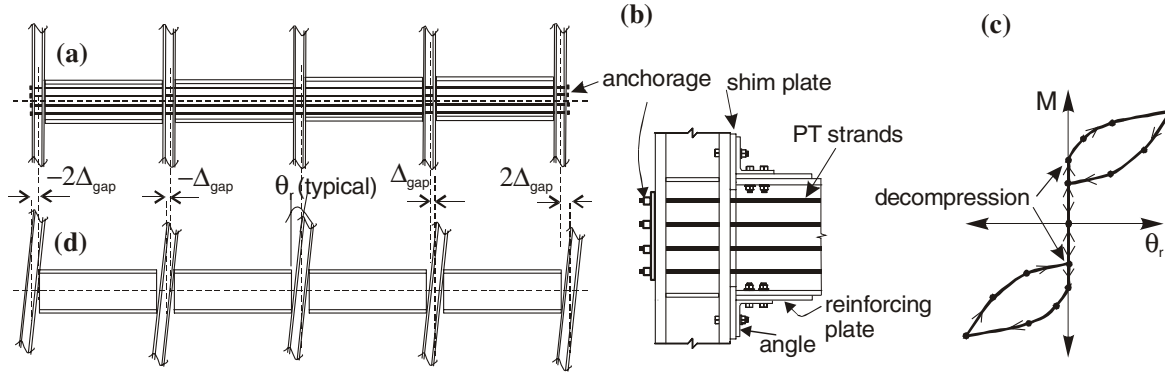
Figure 1. (a) Schematic elevation of one floor of a PT frame, (b) connection details, (c) moment - rotation behavior, and (d) deformed configuration of one floor of a PT frame.

As an alternative to welded connections, the authors developed a post-tensioned (PT) moment connection for use in seismic resistant steel MRFs. The connection utilizes high strength steel strands that are post-tensioned after bolted top-and-seat angles are installed (Figure 1(a)). The post-tensioning strands run through the column, and are anchored against a column flange (Figure 1(b)). The advantages of PT connections and an experimental evaluation of PT connection subassemblies are given in [2,3].

Research on PT MRFs began with precast concrete structures. Cheok and Lew [4] and Cheok and Stone [5] experimentally studied concrete beam-column joint subassemblies with PT connections intended for precast concrete frame structures in seismic zones. They found that the PT concrete joints perform well. El-Sheikh et al. [6] conducted an analytical study of the seismic behavior of unbonded PT precast concrete frames. Recently, post-tensioning has been extended to steel MRFs [7, 8, 9, 10, 11, 12] and steel beams that couple concrete walls [13]. These steel PT systems are all self-centering, however, the details of the PT connections are different. For example, top-and-seat angles, friction devices, and steel bars have been used for energy dissipation, and high strength bars and 7-wire strands have been used for post-tensioning.

The deformation characteristics of PT frames require that special attention be given to the interaction of the PT frame with the *floor system*, which includes the floor slabs, and the floor beams that carry gravity loads and transmit earthquake inertial forces to the PT frame. In the present paper PT *frames* are defined as moment resisting frames (MRFs) with post-tensioned (PT) connections, and PT *frame systems* are PT frames combined with the floor system. The behavior of a PT connection and a PT frame system is described in detail below. This paper proposes a performance based design approach for steel PT frame systems. Seismic performance levels, seismic input levels, structural limit states, and structural demands for a PT frame system are defined. The design objectives are outlined. Design criteria are proposed with the intention of satisfying the design objectives, and a step-by-step design procedure is given. The proposed design approach is evaluated via comparison with time-history analysis results. Although the research presented in this paper was done specifically for PT frames using PT connections with top-and-seat angles (as energy dissipators) and 7-wire strands, the proposed design criteria and design procedure can be extended to PT frame systems with other types of PT connections.
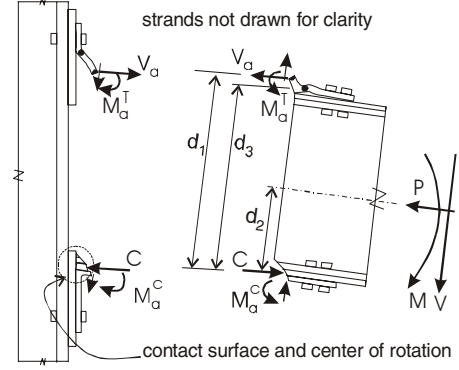
SYSTEM BEHAVIOR

Connection Behavior
The PT steel MRF connection studied consists of bolted top-and-seat angles with seven-wire ASTM A-416 high strength stress relieved strands running parallel to the beam and anchored outside the connection (see Figure 1). The strands compress the beam flanges against the column flanges to resist moment, while the two angles and the friction at the beam - column interface resist transverse shear force. Figure 1(b)

shows a PT connection in an exterior column. The angles dissipate energy and provide redundancy to the force transfer mechanisms for transverse beam shear and moment. Reinforcing plates are welded to the beam flanges to avoid yielding of the flanges. Also, shim plates are placed between the column flange and the beam flanges so that only the beam flanges and reinforcing plates are in contact with the column. The idealized moment-rotation (M-θ_r) behavior of a PT steel connection is shown in Figure 1(c), where θ_r is the relative rotation between the beam and column. The M-θ_r behavior of a PT connection is characterized by gap opening (Δ_{gap}) and closing at the beam-column interface under cyclic loading (Figure 1(d)). The moment to initiate this gap opening is called the decompression moment.

Figure 2. Free body diagram.

The connection initially behaves as a rigid connection (i.e., the initial stiffness of the PT connection is the same as that of a welded connection), but following decompression it behaves as a partially restrained connection. A detailed description of this M-θ_r behavior is given in [8, 9].

A simplified analysis of the behavior of a PT connection can be made using the free-body diagram shown in Figure 2. To make the free body, a cut is made through the fillet of the tension angle (where a plastic hinge forms), the fillet of the other angle, and at the contact surface. It is seen that the beam axial force (P) and the angle forces and moments (V_a, M_a^C and M_a^T) contribute to the moment developed in a PT connection. P is the sum of the PT strand forces (T) and an additional axial force in the PT beams produced by the interaction of the PT frame with the floor system (F_{fd}). F_{fd} is explained in further detail below. P acts at the beam centroid, which is at a distance d_2 from the center of the contact force C. The contact force, C, is assumed to act at the center of rotation. The tension angle force, V_a, is assumed to act at the location of the plastic hinge on the column leg fillet, which is at a distance d_1 from the force C. M_a^C and M_a^T, the moments in the tension angle and compression angle, respectively, act at the plastic hinge locations. Methods for calculating V_a, M_a^C and M_a^T are given in [14].

Horizontal equilibrium requires that C equal the axial force in the beam, P, plus V_a. By summing moments about C, the moment developed in a PT steel connection can be given by the following equation:

$$M = d_1 V_a + P d_2 + M_a^T + M_a^C \tag{1}$$

Decompression occurs when the contact force resultant in the beam tension flange is zero. Assuming V_a, M_a^T, and M_a^C are zero, the decompression moment, M_d, is equal to $d_2 P$, where $P = T_o$ (the total initial post-tensioning force) because F_{fd} is assumed to be zero before the gap opens. Following decompression, the strands elongate producing an increase in strand force, which, in turn, causes the beam to shorten. The total PT force of an interior connection can be shown [9] to be equal to:

$$T = T_o + 2d_2 \left(\frac{k_s k_b}{k_b + k_s} \right) \theta_r \tag{2}$$

where k_s and k_b are the axial stiffnesses (i.e., AE/L) of the strands and beam, L equals the length of one bay, and it is assumed that A, E, L, and d_2 are constant for the entire length of the PT strands.

Interaction of PT Frame with Floor System
The gap opening in a PT connection, which develops after decompression, causes the PT frame to "expand" as shown in Figure 1(d), which is drawn for a four-bay frame. In the deformed position, the distance between the centerline of the columns in a PT frame is larger than it was in the original undeformed position due to the opening of gaps at the beam - column interface. Since the frame and the

floor system are connected, the floor system must also deform. Therefore, it is necessary to examine the interaction between the PT frame and the floor system. Treating the center column as the reference point, and assuming that the gap opening (Δ_{gap}) is unrestrained and the same for all bays, each bay expands a distance Δ_{gap}, and each column moves from the center column a distance $n_b \Delta_{gap}$, where n_b is the number of bays between the column and the center column.

Figure 3 shows one design option that adds flexibility to the floor system. Assuming the inertia force transferred to the PT frame at floor x is F_x, as shown in Figure 3(a), and the building floor plan is as shown in Figure 3(b), the floor system adjacent to the PT frame can be designed to deform as drawn in Figure 3(c) and (d). The shaded areas in these figures indicate areas where composite action is established between the floor slab and the floor beams. Under dynamic loading, the floor inertia forces F_x are transferred to the PT frame via the collector beams, which are the three beams connected to the PT frame shown in Figure 3(d). These collector beams are assumed to behave as shown in Figure 3(c).

In addition to PT strand forces, two additional axial forces develop in the PT frame beams (and thus also in the PT connections) due to the interaction of the PT frame with the floor system:
1. A force, f_x, develops due to the deformation of the collector beams on floor x (seen in Figures 3(c) and (d)). The force from the collector beams "clamps" the PT beams in the interior bays, and produces additional compression forces in the PT frame beams. For the floor system shown in Figure 3, f_x can be estimated as,

$$f_x = \left(K_{cb}\Delta_{gap}\right)_x = \left(K_{cb}d_3\theta_r\right)_x \tag{3}$$

    where K_{cb} equals the stiffness of the collector beam (Figure 3(c)), d_3 is shown in Figure 2, Δ_{gap} is shown in Figure 3 and can be estimated as $d_3\theta_r$, and the subscript indicates floor x.
2. The PT frame beams carry a portion of the floor inertial force, F_x, which is transferred to the PT frames through the collector beams. The collector beams in the 4-bay design in Figure 3 are connected to the three interior columns of the PT frame. Although the exterior columns are not connected to collector beams, they do carry a portion of F_x, which is distributed to the exterior columns via axial forces in the PT frame beams.

The following simplified analysis of the four-bay PT frame in Figure 3 assumes: (1) F_x are distributed to the columns through the collector beams; (2) to reduce the adverse effects of the force f, the center collector beam (connected to the center column) is designed with twice the stiffness of the adjacent collector beams shown in Figure 3(d); (3) the shear in the interior columns are equal to each other, and (4) the shear in an exterior column is equal to one-half the shear of an interior column. These assumptions are based on static pushover analysis results [9] and result in beam axial forces, P_x, which vary as shown in Figure 3(e). $P_x = T_x + F_{fd,x}$, where $F_{fd,x}$ can be expressed as follows:

$$F_{fd,x} = \gamma_1 f_x + \gamma_2 F_x \tag{4}$$

Values of γ_1 and γ_2 can be inferred from Figure 3(e).

It is seen in Figure 3(e) that the beam axial force, P_x, on floor x of a PT frame is not constant across one floor even though the post-tensioned force, T_x, is constant. Equation (1) shows that the connection moment, M, is directly proportional to P. Therefore, M will vary as shown in Figure 3(f), which plots the idealized moment-relative rotation ($M-\theta_r$) behavior of the connections on floor x. For design purposes, the maximum moment in an interior connection and exterior connection must be determined. It has been shown [9] that the variation in the connection moments across each bay of one floor can be significant.
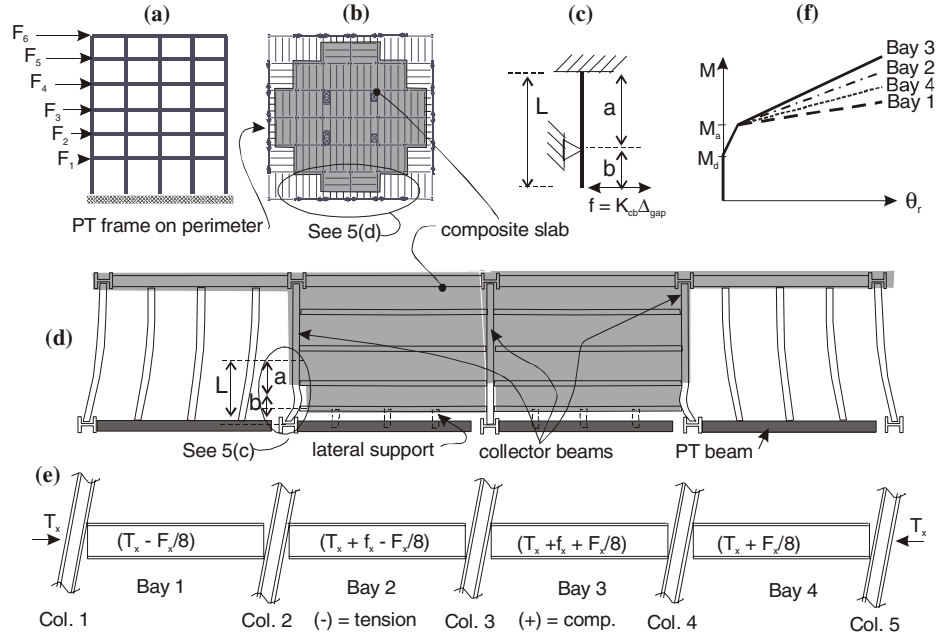
Figure 3. (a) Floor inertia forces on building elevation, (b) plan of hypothetical building, (c) deformation of collector beam, (d) interaction of PT frame with gravity system, (e) beam axial forces (P) on each bay of Floor x, and (f) idealized moment – relative rotation plot of the connection moments on Floor x.

PERFORMANCE-BASED DESIGN APPROACH

Seismic performance is defined by the extent of damage to a structure during an earthquake, and, in turn, the extent of damage is defined by the limit states reached. The extent of structural and non-structural damage defines a *seismic performance level*. The proposed design approach for PT frame systems uses two of the performance levels defined in FEMA-350 [15]: *Immediate Occupancy* (IO) and *Collapse Prevention* (CP). Essentially, the IO performance level is a damage state that does not require structural repair, whereas the CP performance level is a damage state where the structure is on the verge of partial or total collapse.

The *limit states* addressed by the proposed design approach are divided into three categories related to the conformance of the limit state to each performance level as shown in Table 1. Loss of frame self-centering is a limit state that is *not directly* addressed by the proposed design approach; however, self-centering depends on the other limit states reached. Mainly it depends on the extent of beam local buckling, the extent of plastic hinging in the columns, the amount of panel zone yielding, and the amount of strand yielding. Loss of self-centering should not occur at the IO performance level, and should be minimal at the CP performance level.

Table 1. Structural Limit States (LS) Considered by the Design Criteria

LS that conform to IO	LS that do not conform to IO but conform to CP	LS that do not conform to CP
decom-pression; angle yield	collector beam capacity; angle fracture; panel zone yield; column plastic hinge; beam strain = $2\varepsilon_y$; beam yield at column face under bearing stresses; beam horizontal shear yield in the web; story drift and floor system deformation exceed IO limits	beam local buckling; strand yield; excessive drift; excessive floor system deformation.

FEMA-302 [16] provides two specific **seismic input levels** (ground motion intensities) for consideration in design: the *Maximum Considered Earthquake (MCE)* ground motion, and the *Design Basis Earthquake (DBE)* ground motion. **Design objectives** relate the seismic performance levels to the seismic input levels. The proposed design approach has two objectives:

1. Damage to the PT frame system under the DBE must conform to the IO performance level.
2. Damage to the PT frame system under the MCE must conform to the CP performance level.

Figure 4 describes these objectives at the global level using a base shear-roof drift (V - θ_{roof}) plot.
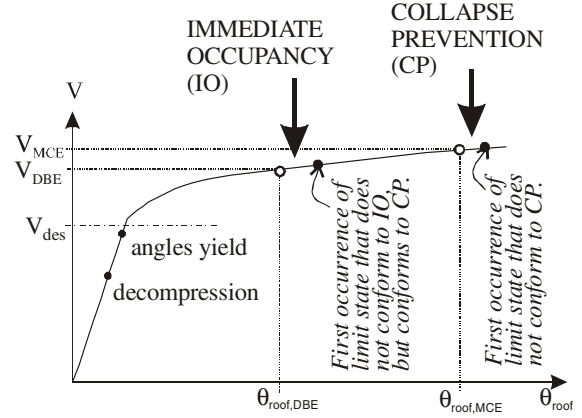
Figure 4. Design objectives related to global response of PT frame.

STRUCTURAL DEMANDS

The structural demands quantify the deformations, forces, and moments in a PT frame system for the DBE and the MCE seismic input levels. The structural demands are used in design criteria that enforce the design objectives defined earlier. In lieu of nonlinear analyses, the structural demands are established as either *capacity based* (i.e., the demands on certain structural components are based on the capacity of the related structural components - such as the strong column-weak beam and panel zone design criteria), *code-based* (i.e., the equivalent lateral force (ELF) procedure in typical US seismic design provisions, which define the story drift - based on linear elastic deflections and a deflection amplification factor, C_d; the design base shear, V_{des}; and the inertial forces acting on a frame at floor x, F_x), or *amplified code-based*. The paragraphs below describe amplified code-based demands.

The actual deformation demands imposed on a PT frame in an earthquake are typically larger than the code-based demands. Therefore, to estimate the roof drift, story drift, and connection relative rotation, θ_r, demands for a PT frame system under the DBE and MCE, an *amplified code-based* procedure is used. This procedure is based on the equal displacement principle, which assumes that the maximum displacement of a nonlinear structure equals the maximum displacement of a linear elastic structure.

Most building codes provide a response spectrum for 5% damping. However, the designer may consider a different level of damping. In this case a damping correction factor (C_ξ) is used to estimate the maximum displacement. The damping correction factor used here is based on a correction factor for smooth response spectra recommended by the Architectural Institute of Japan [17] as follows

$$C_\xi = \frac{\sqrt{1+25\xi_{5\%}}}{\sqrt{1+25\xi}} \tag{5}$$

where $\xi_{5\%} = 0.05$, and ξ is the viscous damping ratio assumed in the design of a PT system.

The ELF procedure is based on the design base shear (V_{des}). However, the period, T_{des}, used to calculate the design base shear may not be the actual fundamental period of the frame. In IBC 2000 [18], for example, T_{des} is the minimum of the actual first-mode period (T_1) and a maximum value defined by the code. In the case where T_{des} is not equal to T_1, a period correction factor (C_T) needs to be applied to estimate the maximum displacement, where

$$C_T = \frac{T_{des}}{T_1} \tag{6}$$

Equation 6 is valid only when V_{des} is a function of $1/T$ as it is in IBC 2000.

Based on the equal displacement principle and these correction factors, the roof displacement demands for the DBE and MCE are estimated as follows

$$\Delta_{roof,DBE} = C_\xi C_T R \Delta_{el-des} \qquad\qquad \Delta_{roof,MCE} = 1.5 C_\xi C_T R \Delta_{el-des} \qquad\qquad (7a,b)$$

where the 1.5 factor for the MCE is based on FEMA-302 [16] definitions of DBE and MCE, R is the response modification factor used to define V_{des} in the ELF procedure, and $\Delta_{el,des}$ is the roof displacement based on an elastic analysis of the frame under the equivalent lateral forces corresponding to V_{des}.

To estimate the *story drift* demand another factor, C_θ, is introduced. C_θ is a constant representing θ/θ_{roof}, where θ is the story drift and θ_{roof} is the roof drift. Based on studies performed by Rojas [19] and Garlock [9] a value of $C_\theta = 1.5$ is recommended. The story drift demands for the DBE and MCE are estimated as

$$\theta_{DBE} = \frac{C_\theta C_\xi C_T R \Delta_{el-des}}{h_f} \qquad\qquad \theta_{MCE} = \frac{1.5 C_\theta C_\xi C_T R \Delta_{el-des}}{h_f} \qquad\qquad (8a,b)$$

where h_f is the total frame height from the ground floor to the roof.

Garlock [9] shows that the beam, column, and panel zone typically remain elastic in a PT frame subject to seismic loading. Therefore if the maximum elastic component of story drift (θ_e) is subtracted from the maximum total story drift (θ), the connection component of story drift remains, which is approximately equal to the maximum relative rotation θ_r (i.e., $\theta_r = \theta - \theta_e$). This is the principle by which the θ_r demand is estimated, and it can be shown [9] that a reasonable approximation for θ_r is

$$\theta_{r,DBE} = \theta_{DBE} - \frac{C_\theta V_{DBE}}{K_{f\Delta} h_f} \qquad\qquad \theta_{r,MCE} = \theta_{MCE} - \frac{C_\theta V_{MCE}}{K_{f\Delta} h_f} \qquad\qquad (9a,b)$$

where $K_{f\Delta}$ is the initial (elastic) frame stiffness equal to the base shear divided by the roof displacement and V_{DBE} and V_{MCE} are the base shear demands for the DBE and MCE (as described below).

Figure 4 shows that the base shear demands for the DBE and MCE (V_{DBE} and V_{MCE}, respectively) are larger than, V_{des}, from an ELF procedure. V_{DBE} and V_{MCE} can be determined directly from nonlinear static pushover analysis results. Alternatively, they can be estimated by the following equations

$$V_{DBE} = \Omega_{DBE} V_{des} \qquad\qquad V_{MCE} = \Omega_{MCE} V_{des} \qquad\qquad (10a,b)$$

where Ω_{DBE} and Ω_{MCE} are overstrength factors for the DBE and MCE, respectively. For PT frames, the values of Ω_{DBE} and Ω_{MCE} are primarily a function of the connection moments at the drift levels corresponding to the DBE and MCE. Typical values of overstrength range from 2 to 3, and Ω_{DBE} is smaller than Ω_{MCE}. Recommendations for Ω are given below.

STRUCTURAL CAPACITIES

Collector beam capacity: If the system is designed as shown in Figure 3, the force causing a plastic hinge to form in the collector beam at a distance *b* from the PT frame (Figure 3c), f_p, equals $M_{cb,p}/b$, where $M_{cb,p}$ is the plastic moment capacity of the collector beam. Based on this relationship and Equation 3, the relative rotation of the PT connections causing the collector beams to form a plastic hinge, $\theta_{r,cb}$, equals

$$\theta_{r,cb} = \frac{M_{cb,p}}{bd_3 K_{cb}} \qquad\qquad (11)$$

Connection moment initiating angle yielding (M_a): M_a can be shown to equal the following [9]:

$$M_a = d_2 T_o + d_1 V_{a,c} \left(1 + \frac{2d_2^2}{K_{a,i} d_1 d_3} \left(\frac{k_b k_s}{k_b + k_s} \right) \right)$$ (12)

where $K_{a,i}$ is the initial stiffness of the angle force-deformation behavior, and $V_{a,c}$ is the angle force when the angle stiffness changes from the elastic to the post-elastic stage. Equations for calculating $K_{a,i}$ and $V_{a,c}$ are given by [14].

Connection moment at the DBE and MCE (M_{DBE} and M_{MCE}): M_{DBE} and M_{MCE} are calculated from Equation 1. Garlock [9] has shown that the contribution of M_a^C and M_a^T to the connection moment is negligible and therefore they can be eliminated for design purposes. Setting P in Equation 1 equal to P_{DBE} (the axial force in the beam under the DBE) and P_{MCE} (the axial force in the beam under the MCE),

$$M_{DBE} = d_1 V_{a,DBE} + P_{DBE} d_2 \qquad\qquad M_{MCE} = d_1 V_{a,MCE} + P_{DBE} d_2$$ (13a,b)

$V_{a,DBE}$ and $V_{a,MCE}$ correspond to the angle force, V_a, when Δ_{gap} equals $d_3 \theta_{r,DBE}$ and $d_3 \theta_{r,MCE}$, respectively. Methods for calculating V_a are described in [14].

It was noted previously that the beam axial forces in floor x, P_x, equal $T_x + F_{fd,x}$. Based on this relationship and Equations 2, 3 and 4, and by setting $F_x = \Omega F_{x,des}$, where $F_{x,des}$ equals F_x corresponding to V_{des}, the beam axial forces for the DBE and MCE, P_{DBE} and P_{MCE}, respectively, can be expressed as

$$P_{DBE} = T_o + \left[2d_2 \left(\frac{k_s k_b}{k_s + k_b} \right) \right] \theta_{r,DBE} + \gamma_1 K_{cb} d_3 \theta_{r,DBE} + \gamma_2 \Omega_{DBE} F_{x,des}$$ (14a)

$$P_{MCE} = T_o + \left[2d_2 \left(\frac{k_s k_b}{k_s + k_b} \right) \right] \theta_{r,MCE} + \gamma_1 \left\{ \begin{matrix} K_{cb} d_3 \theta_{r,MCE} \\ f_p \end{matrix} \right\}_{min} + \gamma_2 \Omega_{MCE} F_{x,des}$$ (14b)

Angle fracture: This limit state is reached in one of two ways; (1) the connection relative rotation reaches $\theta_{r,af}$, which produces angle deformation leading to fracture, or (2) low-cycle fatigue. Assuming that the angles will fracture after about 32 mm of deformation (based on [14]), and assuming that the angle deformation is equal to Δ_{gap}, where $\Delta_{gap} = \theta_r d_3$, then $\theta_{r,af} = 32/d_3$ where d_3 is in units of mm. As indicated by [14], the angles could fracture by low-cycle fatigue. The angles should be evaluated for low-cycle fatigue based on recent research [9, 20].

Strand yield: As the relative rotation in a PT connection increases, the strands continue to elongate. A limit state is reached when the relative rotation reaches $\theta_{r,s}$ causing the strands to yield. $\theta_{r,s}$ is shown [9] to equal the following:

$$\theta_{r,s} = \frac{N_s (t_y - t_o)}{2d_2} \cdot \frac{(k_b + k_s)}{k_b k_s}$$ (15)

where t_y is the force in one strand when it yields, t_o is the initial force in a strand, and N_s is the number of strands. From Equation 15 it can be seen that $\theta_{r,s}$ decreases as the initial force per strand (t_o) increases, and $\theta_{r,s}$ increases as the number of strands (N_s) increases.

DESIGN CRITERIA

To ensure that the performance objectives are satisfied, the design criteria require that the structural *capacities* be greater than the structural *demands* as follows:

Angle yield criterion: For the connection to have sufficient strength, it is recommended that $M_a \geq \alpha_a M_{des}$, where M_{des} is the code-based design moment in the beam at the column face (corresponding to V_{des}) for the controlling load combination, and α_a is a constant selected by the engineer. A practical range for α_a is from 0.75 to 1.0 [9].

Angle fracture criterion: To avoid fracture of the angles under the DBE, $\theta_{r,af} \geq \theta_{r,DBE}$, where $\theta_{r,af}$ is the relative rotation causing angle fracture defined previously, and $\theta_{r,DBE}$ is estimated using Equation 9a. The low-cycle fatigue capacity of the angles also needs to be considered [9, 20].

Strand yielding criterion: For the strands not to yield under the MCE, $\theta_{r,s} \geq \theta_{r,MCE}$, where $\theta_{r,s}$ is the relative rotation causing the strands to yield (given by Equation 15), and $\theta_{r,MCE}$ is estimated using Equation 9b. This criterion ensures that the frame continues to carry gravity load (through friction at the beam – column interface) even if the angles fracture.

Beam local buckling criterion: The strains in the beam should be limited to control flange and web distortion under the MCE, which can lead to local buckling. Therefore, $\theta_{r,bb} \geq \theta_{r,MCE}$. $\theta_{r,bb}$ is the relative rotation causing the beam to buckle locally, and $\theta_{r,MCE}$ is estimated using Equation 9b. It is possible to determine $\theta_{r,bb}$ by a nonlinear finite element analysis. In the absence of such an analysis, beam local buckling under the MCE can be avoided by limiting the beam flange strains at the end of the reinforcing plate to two-times the yield strain ($2\varepsilon_y$) at the DBE. A value of $2\varepsilon_y$ was selected based on subassembly tests of PT connections [2, 9]. From these experiments, it was observed that when the strain exceeded $2\varepsilon_y$, the beam flanges developed significant distortion indicating the onset of beam local buckling. An iterative procedure for determining $\theta_{r,bb}$ is described by [9].

Collector beam strength and stiffness criterion: The details of this section apply only to a four-bay frame with collector beams connected to the three center columns, with the center collector beam being twice as stiff as the two exterior collector beams (as shown in Figure 3). The following criterion does not apply to the center collector beam since theoretically there is no relative displacement between this beam and the center column of the PT frame (as shown in Figure 3d), unless it yields.

If the force causing yielding of the collector beam, f_p, is large relative to the post-tensioning force (T), a permanent gap may remain at the connections of a PT frame. To avoid a permanent gap opening, it is recommended that the total initial PT force, T_o, be greater than f_p. It is also recommended that the collector beam not yield under the DBE, i.e., $\theta_{r,cb} \geq \theta_{r,DBE}$, where $\theta_{r,cb}$ and $\theta_{r,DBE}$ are given by Equations 11 and 9a, respectively. The collector beam must be flexible enough for gap opening to occur, yet rigid enough so that large relative deformations between the floor system and the PT frame do not develop. Research is needed to establish the minimum and maximum collector beam stiffness, although [9] provides some preliminary recommendations.

PT frame story drift criterion: In the proposed design criteria, the story drift limits of seismic design provisions (e.g., [18]) are compared to the ELF procedure elastic analysis results (with the displacements factored by C_d). The *amplified* story drift limits (given below) are compared to the amplified story drift demand estimates given by Equation 8. The recommended amplified story drift limits for PT frames are 0.03 and 0.05 radians for the DBE and MCE, respectively. These limits are based on studies done by [9] and [19] where the performance of PT frames typically did not conform to the IO and CP performance levels if these story drift limits were exceeded.

Column plastic hinge criterion: The strong column-weak beam criterion recommended by current seismic design standards apply to MRFs with fully-rigid connections, which are expected to develop

plastic hinges in the beam near the column face. FEMA-350 [15] equations for ΣM_c (the sum of the column moment *capacity*) and ΣM_b (the sum of the beam moment *demand*) are conservative for PT frames in several ways: (1) the nominal yield stress is used to calculate M_c and a larger stress is used for M_b, (2) M_c does not include the moment contributed by the column shear yet M_b does, and (3) most importantly, FEMA-350 bases M_b on beams with fully-rigid connections, which is significantly larger than M_b for beams with typical PT connections. Therefore, applying FEMA-350 provisions to PT frames results in columns that are larger than necessary. For the beam - column joint in a PT frame, it is recommended that the column capacity and beam demand be defined as follows

$$M_c = Z\left(R_y\sigma_y - \frac{P_u}{A_g}\right) \qquad\qquad M_b = M_{DBE}\frac{L}{L-d_c} \qquad\qquad (16a,b)$$

where R_y is a yield stress modification factor with a value of 1.1, Z is the plastic section modulus, σ_y is the yield stress, P_u is the factored axial load, A_g is the gross cross-sectional area, L is the bay width, d_c is the column depth, and M_{DBE} is the moment developed in a PT connection under the DBE. Equation 16b assumes an inflection point at the beam midspan.

Beam horizontal shear yield criterion: The reinforcing plate length must be long enough to allow horizontal shear to transfer to the web most of the compression (bearing) stresses that are in the beam flange and reinforcing plate at the beam - column interface. The proposed design criterion for beam horizontal shear yield requires that the web horizontal shear stresses at the DBE do not exceed the yield stress. Based on equilibrium of horizontal forces,

$$L_{rp}\tau_{w,y}t_w \geq P_{DBE} + V_{a,DBE} - C_{f,y} \qquad\qquad (17)$$

where $\tau_{w,y}$ is the shear yield stress of the beam web, t_w is the beam web thickness, P_{DBE} is given by Equation 14, and $V_{a,DBE}$ is the angle force at the DBE (calculated based on [14]). The yield force of the beam flange, $C_{f,y}$, equals $b_f t_f \sigma_{f,y}$, where b_f and t_f are the beam flange width and thickness, respectively and $\sigma_{f,y}$ is the flange yield stress.

Beam yield under bearing stresses criterion: This criterion requires that the contact force at the beam – column interface under the DBE, C_{DBE}, does not exceed the total yield force of the reinforcing plate and beam flange, where as described previously $C_{DBE}= P_{DBE} + V_{a,DBE}$. Therefore

$$A_{rp}\sigma_{rp,y} + C_{f,y} \geq P_{DBE} + V_{a,DBE} \qquad\qquad (18)$$

where $\sigma_{rp,y}$ is the yield stress of the reinforcing plate, and A_{rp} is the reinforcing plate area.

Panel zone yield criterion: This criterion controls panel zone yielding under the DBE and is based on the FEMA-350 provisions [15],

$$\phi V_{y,pz} = C_y 0.6\sigma_y R_{yc} d_c t_{pz} \qquad\qquad (19)$$

where $V_{y,pz}$ equals the panel zone shear capacity, σ_y is the nominal yield stress of the panel zone, R_{yc} is the ratio of expected yield stress to the nominal yield stress, equal to 1.1 for Grade 50 steel, d_c is the column depth, and t_{pz} is the panel zone thickness (i.e., the column web thickness plus the doubler plate thickness). C_y is selected by the designer to control the extent of yielding in the panel zone. For $C_y = 1.0$, the panel zones should not yield under the DBE. C_y values less than 1.0 allow some yielding of the panel zones under the DBE. Garlock [9] has shown that for a PT frame the shear demand in the panel zone at the DBE is,

$$V_{pz,DBE} = P_{DBE} - \frac{2M_{DBE}}{h} + 2V_{a,DBE} \qquad V_{pz,DBE} = P_{DBE} - \frac{M_{DBE}}{h} + V_{a,DBE} \qquad (20a,b)$$

(for an interior connection) (for an exterior connection)

DESIGN PROCEDURE

The proposed seismic design procedure for PT frame systems is summarized by the flow chart in Figure 5. The design procedure is iterative, just as it is for the seismic design of any moment resisting frame. Each step of the design procedure is described in detail in [9]. Some details are given below:

- In Step 4, it is recommended that the analysis model include the beam reinforcing plates, rigid offsets for the beam depth and column depth, and panel zone flexibility.
- In Step 6, the structural demands are estimated for the DBE and MCE using the amplified code-based procedure described previously. V_{DBE} and V_{MCE} are determined using overstrength factors Ω_{DBE} and Ω_{MCE}. In the absence of a rigorous analysis, recommended values for Ω_{DBE} and Ω_{MCE} are 1.9 and 2.1, respectively, when $\alpha_a = 0.75$, and 2.2 and 2.5, respectively, when $\alpha_a = 0.95$. These recommendations for Ω_{DBE} and Ω_{MCE} are based on nonlinear dynamic analyses of PT frame systems by [9].
- In Step 7, M_{des} (calculated in Step 4) is multiplied by an α_a factor, which is selected by the engineer (considering the angle yield criterion described previously) to specify the required connection moment at the angle yield limit state.
- In Step 9, the designer chooses C_y, which determines the extent of yielding in the panel zone under the DBE. The required panel zone thickness is calculated using Equations 19 and 20.
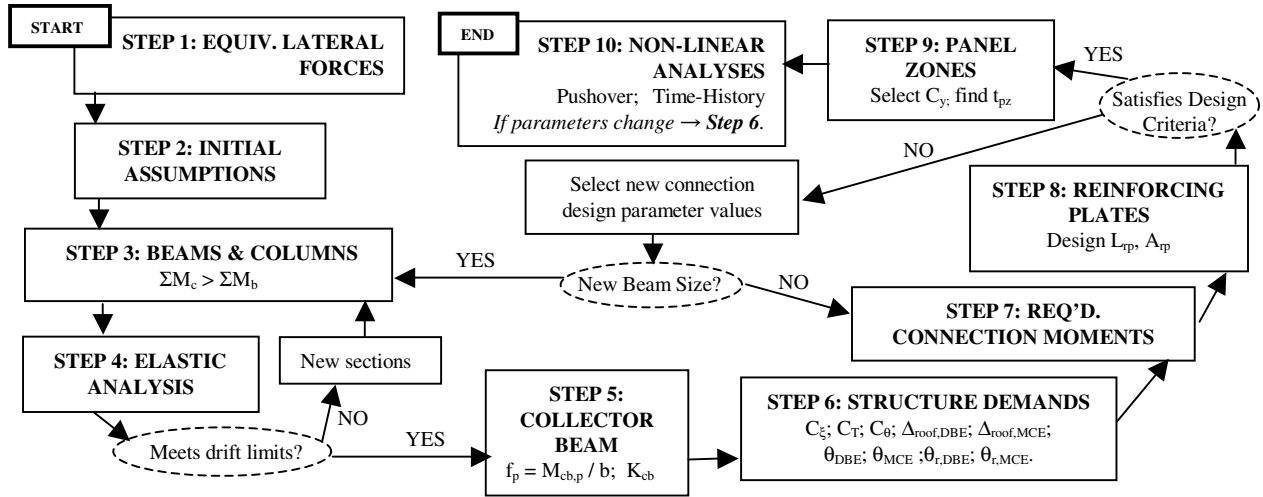

Figure 5. Flow chart for design procedure.

EVALUATION OF DESIGN PROCEDURE

A prototype building designed according to the procedure was evaluated using nonlinear time-history analyses under several ground motions. The design procedure was evaluated by comparing the response from time-history analyses of this prototype building with the *expected* response that is in accordance with the performance objectives. The prototype building, shown in Figure 6, was a 6-story, 6-bay steel office building in the Los Angeles region with 4-bay PT MRFs on the building perimeter. The PT MRF was analyzed using DRAIN-2DX [21]. The details of the analytical model for the prototype building are given by [9]. Two frames were studied, each designed with a different α_a value as shown in Table 2, where Frame A has a larger α_a value than Frame B. In order to strengthen Floors 5 and 6, these floors are designed with larger α_a-values relative to the lower floors. Garlock [9] has shown that designing the upper floors this way improves the performance of frames subject to ground motions that induce a large second mode response. The resulting beam and column sizes, number of strands (N_s), and total initial PT
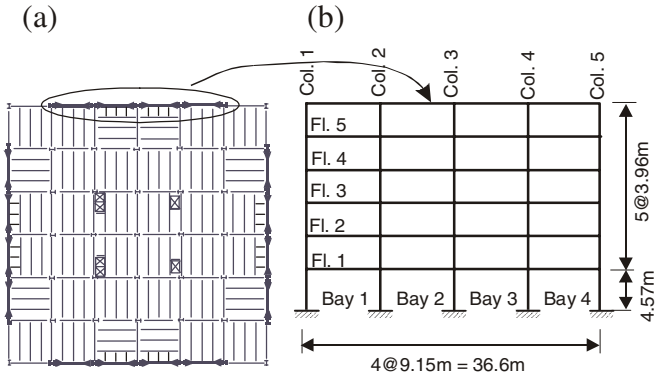
force (T_o) are given in Table 2. The design assumed C_y equal to 1.0 and consequently the interior connections required doubler plates. The reinforcing plate length was 1830 mm on all floors, however the thickness and width varied floor to floor. All the angles were L203x203x19. More details on the prototype building design are presented in [9].

The following three ground motions were used in this study: (1) an *artificial* earthquake ground motion that was generated to be compatible with the IBC 2000 design spectrum [18] (therefore representing the DBE); (2) the 1989 Loma Prieta earthquake ground motion recorded at *Gilroy* Array #3; and (3) the 1995

Figure 6. (a) Plan of prototype building, and (b) elevation of prototype frame.

Kobe earthquake ground motion recorded at the JMA Station. The natural ground motions were scaled according to [22] to a level compatible with the IBC 2000 [18] design spectrum and thus are considered to represent the DBE. The DBE ground motions were multiplied by 1.5 to represent the MCE.

The nomenclature used to identify each analysis (as listed in Table 3) is as follows: (1) the first letter indicates the name of the frame (A or B in this case); (2) the letters following the hyphen represent the ground motion, where *gil*, *kob*, and *art* represent the Gilroy, Kobe, and artificial ground motion, respectively; and (3) the letter in parenthesis indicates the seismic input level that the ground motion was scaled to, where *(D)* represents the DBE, and *(M)* represents the MCE. The time-history analysis results in Table 3 are, where applicable, the <u>maximum</u> within the prototype building. *Average* and *expected* indicates the average of the three time-history results, and the expected <u>maximum</u> response within the prototype building, respectively. The following observations are made by comparing the time-history analysis response to the expected response (see Table 3):

- The expected roof displacement, Δ_{roof}, (Equation 7) is typically larger than the average time-history response. The expected Δ_{roof} is within 22% of the time-history analysis response, with the exception of the Kobe ground motion where the expected value is up to 64% more than the time-history analysis results.

- The expected story drift, θ, (Equation 8) as a percentage of story height (h_x), agrees well with the average time-history response. However, the expected θ exceeds the artificial ground motion response by as much as 50%. Figure 7 plots the maximum and minimum (non concurrent) story drifts at each story of Frame A. It is seen in Figure 7 that the expected θ (for the DBE) provides a reasonable upper bound for all stories. Although not shown, the same trend is seen for the MCE [9].

- The expected connection relative rotation, θ_r, (Equation 9) is up to 35% smaller than the average θ_r from the time-history results, as seen in Table 3.

Table 2. Prototype Frames.

	Floor	Frame A	Frame B
α_a	1-4	0.95	0.75
	5,6	1.2	0.95
Beam	6	W30x90	W24x76
	5	W33x118	W30x108
	4	W36x135	W30x108
	3	W36x170	W36x150
	2	W36x182	W36x160
	1	W36x194	W36x170
Col.	5,6	W14x283	W14x211
	3,4	W14x342	W14x311
	1,2	W14x398	W14x370
N_s; T_o (kN)	6	18; 1361	16; 1352
	5	18; 2002	20; 1779
	4	26; 2139	20; 1957
	3	30; 3136	28; 2366
	2	32; 3558	28; 2865
	1	32; 4199	32; 3131

<p align="center">Table 3. Maximum time-history response and expected response.</p>

Analysis	Δ_{roof} (mm)	θ (%h_x)	θ_r (rad)	$\varepsilon / \varepsilon_y$	Interior Bays P/P_y	$M/M_{p,n}$	Exterior Bays P/P_y	$M/M_{p,n}$
A-gil(D)	653	3.3	0.029	1.9	0.56	1.01	0.52	0.98
A-kob(D)	419	3.1	0.028	1.2	0.52	0.94	0.50	0.92
A-art(D)	503	2.5	0.021	1.3	0.52	0.95	0.50	0.93
average	*526*	*3.0*	*0.026*	*1.5*	*0.53*	*0.97*	*0.51*	*0.94*
expected	*498*	*3.1*	*0.020*	*2.0*	*0.49*	*0.97*	*0.41*	*0.79*
B-gil(D)	638	3.4	0.030	2.2	0.52	1.10	0.45	0.94
B-kob(D)	340	4.2	0.039	3.6	0.57	1.08	0.50	0.98
B-art(D)	584	2.7	0.024	1.3	0.52	0.97	0.49	0.94
average	*521*	*3.4*	*0.031*	*2.4*	*0.54*	*1.05*	*0.48*	*0.95*
expected	*556*	*3.4*	*0.023*	*2.0*	*0.53*	*1.09*	*0.40*	*0.81*
A-gil(M)	914	4.6	0.041	8.7	0.60	1.21	0.56	1.08
A-kob(M)	511	4.2	0.038	2.9	0.57	1.14	0.54	1.02
A-art(M)	747	4.1	0.038	7.2	0.60	1.11	0.56	1.12
average	*724*	*4.3*	*0.039*	*6.3*	*0.59*	*1.15*	*0.55*	*1.07*
expected	*749*	*4.6*	*0.033*	*>2.0*	*0.65*	*1.24*	*0.49*	*0.97*
B-gil(M)	925	5.6	0.051	15.3	0.59	1.27	0.53	1.13
B-kob(M)	546	5.7	0.055	7.2	0.58	1.21	0.57	1.13
B-art(M)	747	3.4	0.033	5.5	0.59	1.11	0.55	1.06
average	*739*	*4.9*	*0.046*	*9.3*	*0.59*	*1.20*	*0.55*	*1.11*
expected	*836*	*5.1*	*0.039*	*>2.0*	*0.71*	*1.39*	*0.50*	*1.05*

Table 3 also lists the following: (1) the beam flange strain, ε, at the end of the reinforcing plate, normalized with respect to the yield strain, ε_y, (2) the beam axial force normalized with respect to the axial force causing yielding of the cross-section (P/P_y) for both the interior bays and exterior bays, and (3) the connection moment normalized with respect to the nominal moment capacity of the beam ($M/M_{p,n}$) for both the interior bays and exterior bays. The $M/M_{p,n}$ and P/P_y values are shown for the interior bays and the exterior bays since the axial forces and moments that develop in the exterior bays are expected to be less than those in the interior bays (see Figure 3). The strain values are only shown for the interior bays, which were larger than the exterior bays with the exception of analysis B-kob(M). Comparing the time-history response to the expected response, the following is observed:
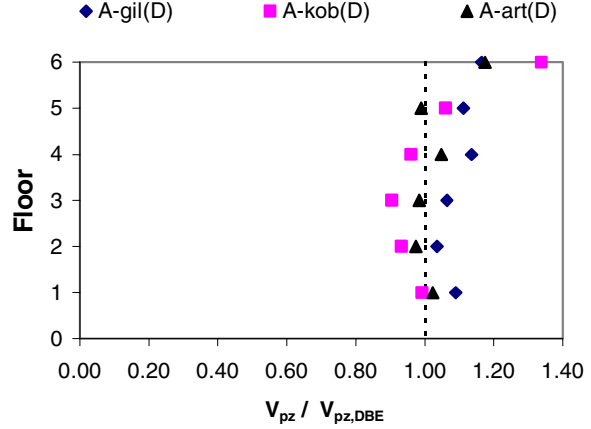
- $\varepsilon/\varepsilon_y$ for the DBE ground motions is relatively close to the value of 2.0 expected by the design procedure. The design procedure does not estimate $\varepsilon/\varepsilon_y$ for the MCE ground motion, although it is implied that the value will be greater than 2.0, which is the case in all time-history results.

- The expected P/P_y and $M/M_{p,n}$ in the *interior* bays (Equations 14 and 13, respectively) correlate better with the time-history results for the DBE than the MCE ground motions. The poorer correlation for the MCE is due to collector beam yielding, which redistributes the horizontal forces in the PT frame (this is not captured in the simplified model).

- The expected P/P_y and $M/M_{p,n}$ (Equations 14 and 13, respectively) in the *exterior* bays underestimate the time-history results. The expected P/P_y are between 6% and 22% less than the time-history results, and the expected $M/M_{p,n}$ are 1% to 19% lower than the time-history analysis results.
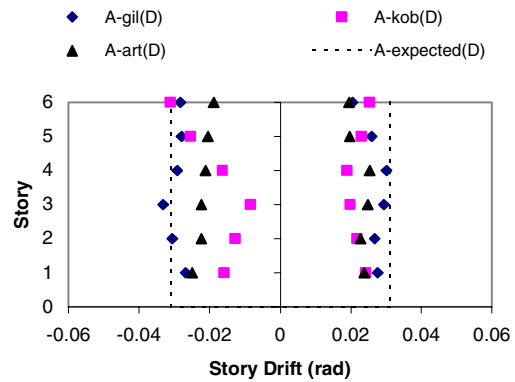
Figure 7. Comparison of predicted story drifts with envelope of time-history results for the DBE ground motions.
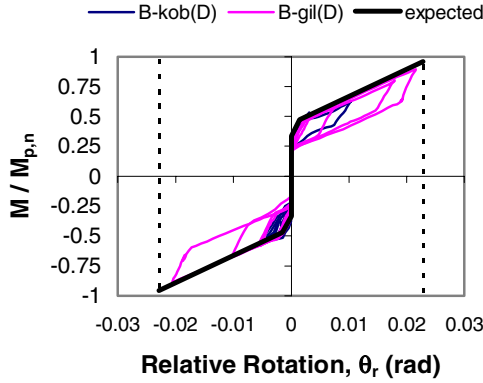
Figure 8. Comparison of expected $M - \theta_r$ response (an *interior* connection, Frame B) with time-history results of the Kobe DBE and Gilroy DBE ground motions.

Figure 9. Ratio of V_{pz} from time-history analyses to estimated panel zone shear ($V_{pz,estim}$) for the *interior* columns of Frame A subject to the DBE ground motions.

The $M/M_{p,n}$-relative rotation (θ_r) response of Frame B, to the Gilroy DBE and Kobe DBE ground motions, is plotted in Figure 8 for an *interior* connection (on Floor 3, Bay 2, right side). Superimposed on this plot is the maximum expected $M/M_{p,n}$ curve for interior bays based on Equation 13. The expected curve extends only to the maximum expected $\theta_{r,DBE}$ (Equation 9). It can be seen that the time-history moment - rotation response is stable and agrees well with the expected results. The same trend is seen for exterior connections [9].

Garlock [9] shows that the expected panel zone shear demand (based on Equation 21) provides a reasonable estimate of the panel zone shear demand in the interior and exterior connections. As an example, Figure 9 plots the ratio of maximum panel zone shear (V_{pz}) from time-history analyses to the expected panel zone shear demand (Equation 21) ($V_{pz,DBE}$) for the interior columns of Frame A subject to the DBE ground motions. It is seen that the correlation is good between the expected demands and the time-history results.

Garlock [9] examines the conformance of the prototype frame performance to the design objectives by looking at the limit states reached in each time-history analysis. It was observed that both Frame A and Frame B satisfied the design criteria for the limit states of decompression, angle yield, angle fracture, and strand yield. Furthermore, small, if any, residual displacements existed at the end of the analyses, which agrees with the design intent. The other design objectives were not always satisfied for a few beams and columns in the frame. Typically, however, Frame A came closer to conforming to the design objectives than Frame B. A more detailed comparison between the response of Frame A and B is given in [9].

SUMMARY AND CONCLUSIONS

The behavior of a PT connection and PT frame system has been described, where a PT frame system is a PT frame interacting with the floor system. It has been shown that the gap opening in the PT connections, which develops after decompression, causes the PT frame to "expand", and the floor system must be flexible enough to permit this gap opening to occur. However, the floor system partially restrains the gap opening, and produces axial forces in the beams that add to the axial forces produced by the post-tensioning. These additional axial forces vary across the PT frame and cannot be neglected.

This paper proposed a performance based design approach for steel PT frame systems. Seismic performance levels, seismic input levels, structural limit states, and the structural demands for a PT frame system were defined. The design objectives were outlined and design criteria were proposed with the intention of satisfying the design objectives. A step-by-step design procedure was given for PT frame systems.

The seismic behavior of steel PT frame systems, designed according to the procedure described in this paper, was investigated to evaluate the design approach. The expected structural demands were compared to the time-history results. The expected story drift demand provides a good upper bound while the expected connection relative rotation underestimates the demand on some floors. Typically, the expected maximum P/P_y and $M/M_{p,n}$ in the *interior* bays slightly overestimate the time-history results, where the maximum expected P/P_y and $M/M_{p,n}$ in the *exterior* bays slightly underestimate the time-history results. PT frames designed using the proposed design approach satisfied the design criteria for the limit states of decompression, angle yield, angle fracture, and strand yield. The other design criteria were not always satisfied by a relatively few number of beams or columns in the frame.

ACKNOWLEDGEMENTS

REFERENCES

1.   Roeder, C.W. "State of the Art Report Connection Performance," Federal Emergency Management Agency (FEMA) *Bulletin No. 355D*, Washington, D.C., 2000.
2.   Garlock, M, Ricles, J., and Sause, R. "Experimental Studies on Full-Scale Post-Tensioned Steel Connections" (submitted to *Journal of Structural Engineering* in Nov. 2003).
3.   Garlock, M, Ricles, J., and Sause, R. "Experimental Studies on Full-Scale Post-Tensioned Steel Moment Connections", *Proceedings of 13th World Conference on Earthquake Engineering*, Vancouver, B.C., Canada, August 2004.
4.   Cheok, G. and Lew, H.S. "Model Precast Concrete Bean-to-Column Joints Subject to Cyclic Loading," *PCI Journal*, Precast/Prestressed Concrete Institute, v. 38, No. 4, July-August 1993: 80-92.
5.   Cheok, G. and Stone, W. "Performance of 1/3-Scale Model Precast Concrete Beam-Column Connections Subjected to Cyclic Inelastic Loads – Report No. 4," *NISTIR 5436*, National Institute of Standards and Technology, NIST, Gaithersburg, MD, June 1994.
6.   El-Sheikh, M.T., Sause, R., Pessiki, S., and Lu, L.-W. "Seismic Behavior and Design of Unbonded Post-Tensioned Precast Concrete Frames," *PCI Journal*, 44 (3), May/June 1999: 54-71.
7.   Ricles, J., Sause, R., Peng, S.W., and Lu, L.W. "Experimental Evaluation of Earthquake Resistant Posttensioned Steel Connections," *Journal of Structural Engineering,* ASCE, 128(7), 2002: 850-859.
8.   Ricles, J., Sause, R., Garlock, M, and Zhao, C. "Post-Tensioned Seismic Resistant Connections for Steel Frames," *Journal of Structural Engineering,* ASCE, 127(2), 2001: 113-121.

9. Garlock, M. "Full-Scale Testing, Seismic Analysis, and Design of Post-Tensioned Seismic Resistant Connections for Steel Frames," *Ph.D. Dissertation*, Civil and Environmental Engineering Dept., Lehigh University, Bethlehem, PA., 2002.

10. Christopoulos, C., Filiatrault, A., Uang, C.-M., Folz, B." Posttensioned Energy Dissipating Connections for Moment-Resisting Steel Frames", *Journal of Structural Engineering,* ASCE, 128(9) 2002: 1111-1120.

11. Christopoulos, C., Filiatrault, A., and Uang, C.-M. "Behavior of Steel Moment Resisting Frames with Post-Tensioned Energy Dissipating Connections," in *Proceedings of the 7th U.S. National Conference on Earthquake Engineering (NCEE)*, Boston, MA 2002.

12. Christopoulos, C., Filiatrault, A., and Uang, C.-M. "Seismic Demands on Post-Tensioned Energy Dissipating Moment-Resisting Steel Frames," in *Proceedings of Steel Structures in Seismic Areas (STESSA)*, Naples, Italy 2003.

13. Shen, Q., and Kurama, Y.C. "Nonlinear Behavior of Hybrid Coupled Wall Subassemblages", *Journal of Structural Engineering,* ASCE, 128(10) 2002: 1290-1300.

14. Garlock, M, Ricles, J., and Sause, R. "Cyclic Load Tests and Analysis of Bolted Top-and-Seat Angle Connections," *Journal of Structural Engineering*, ASCE 129(12), 2003: 1615-1625.

15. *Recommended Design Criteria For New Steel Moment Frame Structures. Report No. FEMA-350*, prepared by the SAC Joint Venture for the Federal Emergency Management Agency (FEMA), Washington, D.C., 2000.

16. NEHRP Recommended Provisions for Seismic Regulations for New Buildings and Other Structures, Part 1 – Provisions. Report No. FEMA-302, 1997, prepared by Building Seismic Safety Council for the Federal Emergency Management Agency, Washington, D.C.

17. *AIJ Recommendations for the Design of Base Isolated Buildings*. Architectural Institute of Japan, Tokyo, Japan, 1993.

18. *International Building Code*. International Code Council, Falls Church, Virginia, 2000.

19. Rojas, P. "Seismic Analysis and Design of Post-Tensioned Friction Damped Connections for Steel Frames", Ph.D. Dissertation, Department of Civil and Environmental Engineering, Lehigh University, Bethlehem, Pa., May 2003.

20. Kasai, K., and Xu, Y. (2003). "Cyclic Behavior and Low-Cycle Fatigue of Semi-Rigid Connections (Part I: Bolted Angle Connections)", in *Proceedings of Steel Structures in Seismic Areas (STESSA)*, Naples, Italy.

21. Prakash, V., Powell, G., and Campbell, S. "DRAIN-2DX Base Program Description and User Guide; Verion 1.10," Report No. UCB/SEMM-93/17&18, Structural Engineering Mechanics and Materials, Department of Civil Engineering, University of California, Berkeley, CA, December, 1993.

22. Somerville, P., Smith, N., Punyamurthula, S., Sun, J., and Woodward-Clyde Federal Services.*Development of Ground Motion Time Histories for Phase 2 of the FEMA/SAC Steel Project*. SAC/BD-97/04 SAC Joint Venture, 1997.